ISSN 1068-3356, Bulletin of the Lebedev Physics Institute, 2023, Vol. 50, Suppl. 5, pp. S560–S571. © Allerton Press, Inc., 2023.
Russian Text © The Author(s), 2023, published in Kvantovaya Elektronika, 2023, Vol. 53, No. 1, pp. 34–42.

INTERACTION OF LASER RADIATION WITH MATTER. LASER PLASMA

HTSC Maglev Ring System for Noncontact Acceleration and Injection of Cryogenic Fuel Targets into the Laser Focus of an ICF Facility

I. V. Aleksandrova[a], A. A. Akunets[a], S. Yu. Gavrilkin[a], V. D. Zvorykin[a], O. M. Ivanenko[a], E. R. Koresheva[a,*], E. L. Koshelev[a], K. V. Mitsen[a], A. I. Nikitenko[a], T. P. Timasheva[a], and A. Yu. Tsvetkov[a]

[a] *Lebedev Physical Institute, Russian Academy of Sciences, Moscow, 119991 Russia*

**e-mail: elena.koresheva@gmail.com*

Received September 5, 2022; revised November 27, 2022; accepted November 27, 2022

Abstract—Creation of an efficient system for the frequent delivery of cryogenic fuel targets (CFT) to the focus of a powerful laser facility is one of the key directions of research in inertial confinement fusion (ICF). The paper discusses prospects for the creation of a ring magnetic system based on the contactless acceleration of a levitating CFT carrier made of high-temperature type II superconductors (HTSC), up to specified injection velocities of 200–400 m/s. For this purpose, the temperature dependence of the magnetic moment of HTSC tapes in the range $\Delta T = 10$–92 K was studied, prototype experiments on the acceleration of HTSC carriers at $T \sim 80$ K due to an external action on them with a frequency of ~1 Hz were carried out, and the speed for the stall of HTSC carriers from a circular trajectory were calculated. The calculation results are in good agreement with the experiment, which makes it possible to estimate the parameters of the ring magnetic accelerator for the operating temperature of the CFT injector $T \sim 17$ K. It is shown that the method proposed is promising for the creation of systems for noncontact delivery of CFT based on the principles of levitation and subsequent injection of CFTs into the center of the ICF reactor chamber at the required speed. The results of planning a new series of experiments are presented: acceleration of an HTSC carrier followed by injection of a surrogate target into the chamber of the GARPUN (LPI) KrF laser.

Keywords: nertial confinement fusion (ICF), cryogenic fuel target (CFT), contactless CFT delivery, high-temperature superconductors (HTSC), magnetic levitation (maglev)

DOI: 10.3103/S1068335623170025

1. INTRODUCTION

Creation of a system for frequent delivery of unsuspended cryogenic fuel targets (CFT) to the thermonuclear fusion zone of a high-power laser facility or a future reactor is one of the key tasks in planning and implementing experiments on inertial confinement fusion (ICF) [1]. A specific feature of the delivery process lies in the requirements for the frequency of delivery (5–10 Hz), its accuracy, and temperature conditions. A CFT should be positioned in the center of the chamber with an accuracy of ±5 mm. In this case, the accuracy of alignment of the laser beams and the CFT in the final position is ±20 μm. A spherical CFT (the outer diameter of the reactor CFT does not exceed 4 mm, the mass is less than 4.5 mg) at the moment of laser irradiation should have a temperature not higher than 18.3 K [2]. In this case, the temperature of the reactor chamber wall can reach significant values. For example, for the designed chamber of the SOMBRERO reactor, the wall temperature is 1758 K [1]. Permissible overloads on a CFT during its acceleration in the injector can be from 500*g* to 1000*g* [3]. Therefore, the acceleration of a CFT is carried out in a special carrier capsule. This carrier transfers the momentum of the motion to the CFT as it is accelerated to the required injection velocities of 200–400 m/s [3].

The choice of the CFT accelerator type is one of the main problems in the practical implementation of the above requirements. Therefore, in the leading laboratories of the world, various traditional approaches for accelerating and injecting CFTs are being studied; among them are pneumatic and electromagnetic guns and electrostatic and gravitational injectors [4–9]. However, in the traditional approach, during CFT acceleration, the friction of the CFT carrier against the wall of the injector guide tube results in heat release, which can lead to overheating of the CFT above the permissible limit (~100 mK) and loss of qual-

ity of the fuel layer [8]. In addition, with the traditional approach, there is a risk of disruption of the injector due to wedging of the carrier in the guiding tube [9].

Thus, maintaining the quality of the fuel layer, reducing risks during the operation of the injector, and ensuring the frequent delivery of CFTs to the thermonuclear fusion zone requires the creation of a noncontact accelerator that excludes mechanical friction. This is also important from another point of view: it removes one of the critically important issues, namely, the necessity of the development of cryogenic lubricants, the effectiveness of which at cryogenic temperatures (below 20 K) is highly questionable. One possible solution is to use superconductor levitation in a magnetic field (maglev). Since the CFT temperature at the time of laser irradiation should be ~18.3 K, low-temperature type I superconductors with superconducting transition temperatures $T_c < 9$ K are not suitable for solving the formulated problem.

At the Lebedev Physical Institute of the Russian Academy of Sciences (LPI), an original method for non-contact acceleration of CFTs was proposed, tested, and patented; it is based on the use of the quantum levitation effect of type II high-temperature superconductors (HTSC) in a gradient magnetic field [10–15]. Special attention is paid to the creation of special magnetic guide systems, linear or cyclic. As a material for the CFT carrier, it is proposed to use HTSCs with a critical temperature higher than 90 K, which makes it possible to accelerate an HTSC carrier with a CFT at the required temperatures (~17 K) and completely exclude the contact of the carrier with the accelerator guide tube due to levitation of the carrier in magnetic field (magnetic levitation, maglev). Of great importance from both scientific and technological points of view is the fact that such a maglev transport [16] provides fast acceleration of an HTSC carrier using a traveling magnetic wave formed by a series of solenoids [14]. After reaching the required injection velocity of the CFT, the HTSC carrier is decelerated in the electromagnetic field of the solenoid, and the CFT is separated from the carrier by inertia and injected into the ICF chamber.

Previously, we have shown the fundamental possibility of constructing a linear accelerator for implementing contactless delivery of CFTs to the focus of a powerful ICF facility [10–12]. The main elements of such an accelerator are a linear magnetic system (linear magnetic rail or track), a solenoid mounted along the magnetic rail, and an HTSC carrier. The movement was started with the help of a short solenoid, which created a short-term magnetic pulse acting on the HTSC carrier. Since all superconductors are diamagnets, they are pushed out of the region of a strong magnetic field, and thus the HTSC carrier is accelerated by a magnetic pulse.

The results of experimental and theoretical modeling showed that a linear accelerator can be built for the entire range of injection velocities (200–400 m/s) and, for the maximum velocity $v_{inj} = 400$ m/s, the acceleration length L_a is 20 m at accelerations $a < 500g$. An important fact is that the acceleration using a traveling magnetic wave in a linear system will require a significant number of solenoids (more than 100) located along the entire magnetic rail.

If the CFTs have sufficient mechanical strength, another acceleration scenario can be realized, with $v_{inj} = 400$ m/s, $L_a = 10$ m, and $a = 800g$ (which is less than the maximum allowable accelerations ~$1000g$). After reaching the required speed, the HTSC carrier will separate from the CFT due to its deceleration in the magnetic field of the solenoid (HTSC is a diamagnet), and the CFT (non-magnetic projectile) will continue to move by inertia.

At the moment, LPI successfully conducts research on the creation of magnetic systems of the HTSC maglev type for operation not only in a linear acceleration scheme, but also in a closed version for the so-called cyclotron acceleration method [13–15]. The use of a ring or an oval magnetic system is promising from the viewpoint of reducing the linear dimensions of the accelerator, as well as reducing the number of accelerating solenoids from 100 to 2–4. At the same time, we considered the basic principles for constructing a closed magnetic system and carried out the first successful experiments. In particular, when using only one solenoid in an oval magnetic system (size 22 × 9.5 cm), the increase in the speed of the HTSC carrier was ~1 m/s per revolution (a model experiment was carried out at $T \sim 80$ K) [14].

In this paper, we present the results of new prototype experiments on noncontact acceleration of an HTSC carrier in a ring magnetic system (MS-4a type) under an external frequency action in the range of ~1 Hz. By measuring the velocity, acceleration, and temperature characteristics of the HTSC material used in various magnetic fields, we studied the dynamic stability of the movement of an HTSC carrier in the MS-4a system with the aim of passing from model experiments in the temperature range ~80 K to the creation of a prototype of a closed CFT accelerator working at the operating temperature of the injector $T \sim 17$ K.

Fig. 1. (a) General view of the measuring complex PPMS-9 (Quantum Design), (b) HTSC tape manufactured by SuperOx, and (c) levitation of a HTSC tape in a magnetic field at $T \sim 80$ K.

2. PREPARATION OF THE EXPERIMENT

2.1. Measuring the Magnetic Moment of HTSC Samples

To compare the calculated and experimental results on the acceleration of an HTSC carrier at different temperatures and in different magnetic fields, it is necessary to know the temperature dependence of the magnetic moment of the HTSC tape from which the HTSC carrier is made. We used a SuperOx J-PI12-20Ag-20Cu HTSC tape consisting of an Ag layer (2 μm thick), a Cu layer (20 μm) with a Hastelloy substrate, and a layer of nonmagnetic material C-276 (60 μm). Unfortunately, we failed to find in the scientific literature the necessary data for this material in the temperature range of our interest, 10–92 K, with the required measurement step of about 1600 temperature points for each value of magnetic induction varying in the range 0.01–8.0 T. For this reason, we carried out our own measurements of the magnetic moment of the HTSC tape for the following parameters [17]: density $\rho = 3.25$ g/cm^3, critical current $I_c = 150$ A at 77 K, critical magnetic field $B_c > 45$ T at 0 K, and temperature $T_c = 92$ K. The measurements were carried out under the indicated conditions on a multifunctional setup PPMS-9 (Quantum Design) (Fig. 1a) with the following characteristics:

– the range of the magnetic field used in the measurements of ±9 T with a field uniformity not worse than 0.01%;

– the range of temperatures available during measurements of 0.35–400 K with an accuracy of maintaining the temperature not worse than 0.01 K;

– the accuracy of measurements of the magnetic moment of $\pm 2.5 \cdot 10^{-5}$ G · cm^3.

The measurement results obtained are shown in Fig. 2. The temperature dependence of the magnetic moment of the HTSC sample ($M = \chi H$, where H is the magnetic field strength and χ is the magnetic susceptibility of the sample) was measured in various magnetic fields in the zero-field cooled (ZFC) mode. When implementing the ZFC mode, the sample under study—a segment of the HTSC tape (see Figs. 1b and 1c)—was cooled to 10 K in zero field, after which a constant magnetic field was switched on and the temperature slowly increased to a superconducting transition temperature T_c and above (for the SuperOx HTSC tape, $T_c = 92$ K). The measurements were carried out at $B = 0.01$, 0.5, 1.0, 2.0, 4.0, and 8.0 T. The measurements were performed at about 1600 temperature points at each value of the magnetic field.

For a detailed analysis of the results obtained, the data of measurements of the magnetic moment in the temperature range 10–85 K for the magnetic fields of our interest (1 and 2 T) are summarized in Table 1. A fact important for the subsequent discussion is that the modulus of M increases by 1–2 orders of magnitude as the temperature decreases from 85–80 to 17 K. In particular, at $B = 1$ T, a decrease in temperature from 80 to 17 K leads to an increase in the modulus of M by 44 times; a decrease from 83 to 17 K, to its increase by 114 times; and a decrease from 85 to 17 K, to an increase by 413 times.

2.2. Ring Magnetic System

To implement the cyclotron acceleration method, an MS-4a ring magnetic system (Fig. 3a) was created, the main element of which is a ring magnet (Midora) made of NdFeB neodymium alloy with a Ni–Cu–Ni anticorrosion coating (axial magnetization); the outer and inner diameters of the magnet

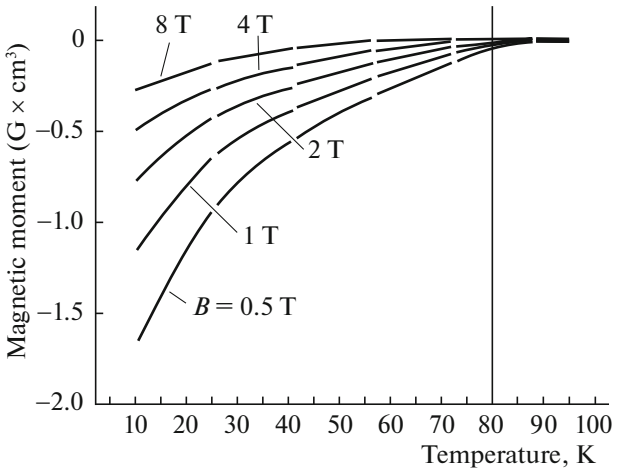

Fig. 2. Results of measuring the magnetic moment of SuperOx HTSC tape at the PPMS-9 facility.

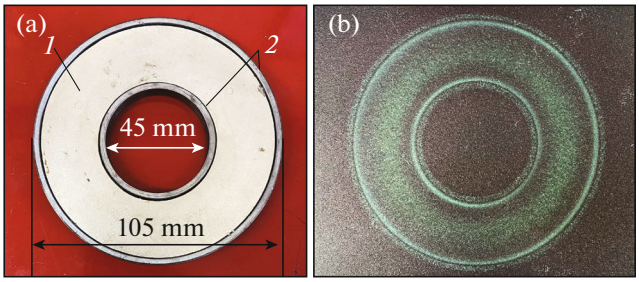

Fig. 3. Ring magnetic system MS-4a: (a) top view (*1* – magnet, *2* – ferromagnetic insert); (b) magnetic field configuration obtained using a visualizing film.

are 100 and 50 mm, respectively, the height is 5 mm, the magnetic induction is $B = 0.13–0.25$ T, and the weight is 218 g. The magnet is fixed inside a ferromagnetic insert (produced by LPI) made of ARMKO soft magnetic iron (outer and inner diameters 105 and 45 mm, height 7.5 mm, depth of the trough for the magnet 5 mm). Such an insert makes it possible to create the required gradient of the magnetic field (the so-called magnetic wall) at the edges of the system.

The principle of constructing various magnetic systems, the choice of superconducting materials, and experimental and theoretical modeling of the functional features of the transport of levitating HTSC carriers are discussed in detail in [15]. Here, we only emphasize the fact that the stable motion of an HTSC carrier is ensured by placing it in a gradient magnetic field and, if the magnetic field has a certain symme-

Table 1. The results of measuring the magnetic moment of an HTSC tape sample (SuperOx) with dimensions of 4 mm × 4 mm × 120 μm

T (K)	$\|M\|$ (G cm^3)	
	$B = 1$ T	$B = 2$ T
10	1.14022	0.75999
17	0.88404	0.58325
18	0.83826	0.55392
20	0.78202	0.51457
80	0.02	0.00209
83	0.00772	0.00269
85	0.00214	0.00384

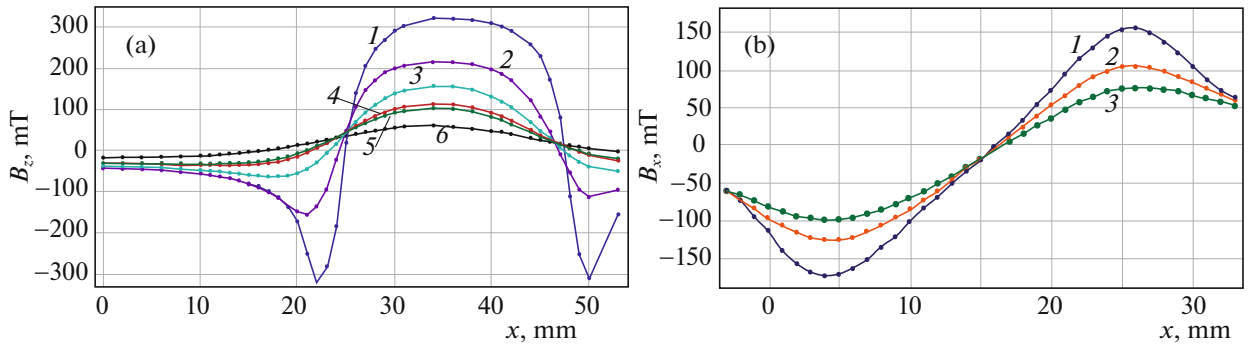

Fig. 4. Results of measuring the magnetic field of the MS-4a ring magnetic system: (a) vertical z-component of the field (B_z) at the levitation height h = (*1*) 1, (*2*) 4, (*3*) 7, (*4*) 10, (*5*) 11, and (*6*) 16.5 mm; (b) horizontal x-component of the field (B_x, directed along the radius r) at the height h = (*1*) 6, (*2*) 8, and (*3*) 10 mm.

try, linear or circular, then the motion is carried out along the lines of symmetry of the magnetic field. In all other directions, the superconductor is a kind of locked up due to the quantum capture of the superconductor in a magnetic field [18, 19]. This fixation of the superconductor in height and orientation suppresses unwanted vibrations in the system, stabilizing the process of linear or cyclic acceleration. This opens the way to the creation of a magnetic rail for the transport of an HTSC carrier using levitation. In other words, in the presence of a strong gradient of the magnetic field in one direction and no gradient in any other direction, an HTSC carrier can exhibit stable levitation over a magnetic rail, moving freely back and forth along the rail in the direction of zero gradient of the magnetic field (see formula (1) in Section 3).

Figure 3b shows the configuration of the magnetic field, obtained using a visualizing film, which makes it easy to map magnetic fields and radiation patterns on the surface of a magnet or magnetic assembly. This figure demonstrates the circular symmetry of the magnetic field of MS-4a. This means that the magnetic flux does not change along the circular rail, allowing the HTSC carrier to move freely around the circumference. In all other directions, it will be blocked due to the radial gradient of the magnetic field that exists across the rail (characteristic light lines in Fig. 3b).

The results of measuring the characteristics of the magnetic field of the MS-4a system are shown in Fig. 4. The measurements were carried out using an MF-1 NOVOTEST magnetometer based on a DKhK-0.5A Hall sensor with a sensitivity of 280 mV/T. The measurement range was ±250 mT, the absolute measurement error was ±5 mT, and the positioning accuracy of the sensitive element was 0.1 mm.

An HTSC carrier can be accelerated by both magnetic and mechanical action on the carrier. In this work, we used a single mechanical action or a variable load that occurs due to a change in the angle of inclination of the MS-4a surface, since this makes it possible to most simply and clearly study such parameters of the ring magnetic system as guidance (trajectory control), levitation rate, and stability.

In the experiments, we used two prototypes of HTSC carriers made from the SuperOx superconducting tape. Design options for these carriers are shown in Fig. 5. When moving in the MS-4a ring magnetic system, the number of turns at the same levitation height depends on the heating rate of the HTSC from $T \sim 80$ K to a temperature near the superconducting transition $T_c = 92$ K. To avoid rapid heating, simple insulating materials and some combinations of them are traditionally aluminum foil, liquid nitrogen (boiling point 77 K), or polymer foam impregnated with liquid nitrogen (Fig. 6). In the discussed series of experiments, for prototype 1 (an open parallelepiped), liquid nitrogen was poured directly into the carrier (Fig. 5b and 6a) and, for prototype 2 (a closed parallelepiped), polymer foam impregnated with liquid nitrogen and located inside the case of the carrier (Fig. 6b). This approach to the choice of the carrier geometry and the method of thermal insulation makes the set up of experiments more convenient and practical for any form of a closed magnetic system: oval (Fig. 6) or circular (Fig. 7). Note that, for prototype 1, the use of polymer foam is also possible.

Before proceeding to a discussion of a new series of experiments on the frequency acceleration of an HTSC carrier, let us consider its motion under conditions of a single external action. In this case, an HTSC carrier (prototype 1, Fig. 7a) was placed above the MS-4a system and set in motion by a simple mechanical push. Still images of its rotation at $T \sim 80$ K are shown in Figs. 7b–7d. To demonstrate the stability of the levitation process, we used prototype 1 (mass 1.25 g) with an additional load in the form of two cylinders weighing 1.1 g each. For comparison, we recall that the mass of the reactor CFT is less than

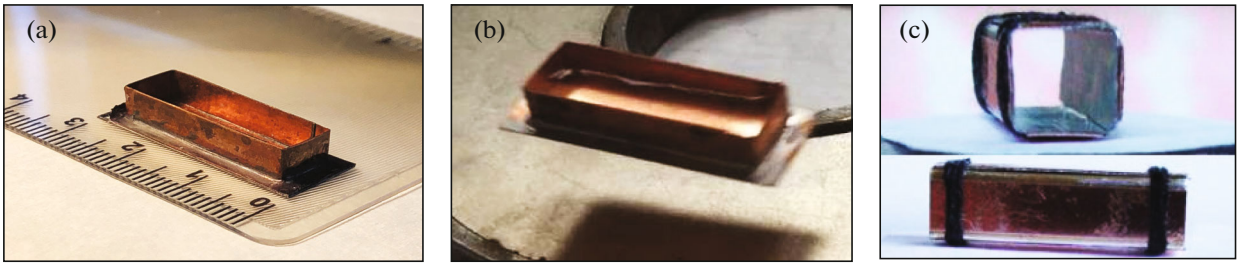

Fig. 5. (a) Experimental prototypes of HTSC carriers: prototype 1 (substrate dimensions 30 × 12 mm, internal dimensions 8 × 5 × 4 mm, $T = 300$ K); (b) prototype 1 with liquid nitrogen inside ($T \sim 80$ K); (c) prototype 2 (dimensions 13 × 4 × 4 mm, $T = 300$ K).

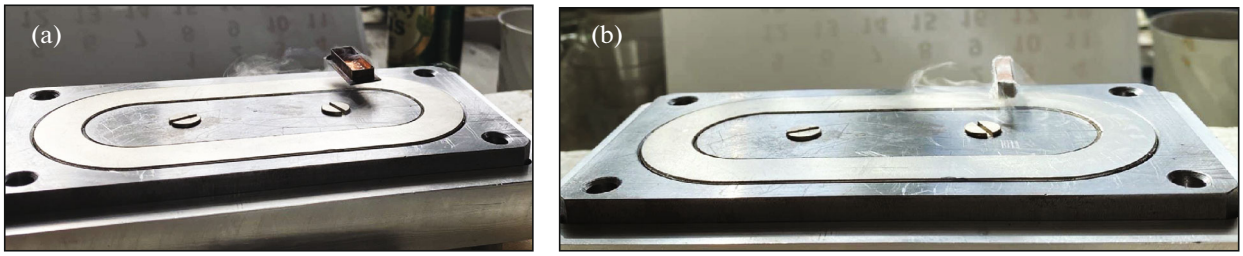

Fig. 6. Methods for stabilizing the temperature of HTSC carriers: (a) prototype 1 (weight ~1.25 g) in the form of an open parallelepiped with liquid nitrogen inside; (b) prototype 2 (weight ~1 g) in the form of a closed parallelepiped with polymer foam impregnated with liquid nitrogen and located inside the carrier body.

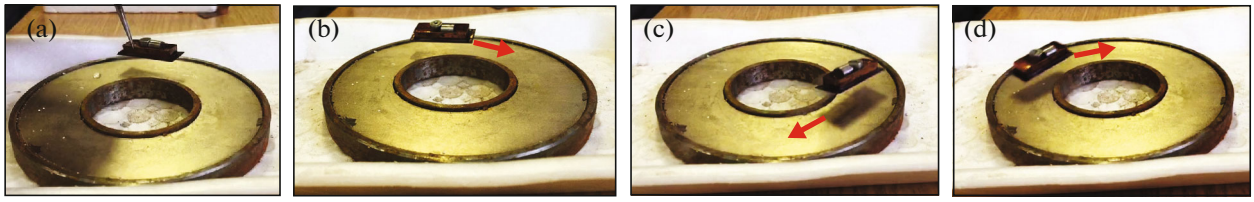

Fig. 7. Freeze-frames of the rotation of the HTSC carrier (prototype 1 with two cylinders) in the MS-4a system at $T \sim 80$ K after a single mechanical impact.

4.5 mg [2]; i.e., structurally, the mass of the HTSC carrier itself depends only on the conditions for implementing the required parameters of the acceleration process (see Sections 3 and 4). A fact important for us is that, after a single shock (Fig. 7a), which sets the speed of movement, the trajectory of the HTSC carrier, including not only the radius of the orbit, but the speed and height of levitation, remained unchanged; i.e., the movement was stable until the moment of significant heating of the HTSC.

3. SIMULATION OF THE OPERATION OF THE HTSC MAGLEV SYSTEM FOR NONCONTANCT ACCELERATION OF CFT

Figure 8 shows a schematic of conducting a new series of experiments under conditions when an HTSC carrier receives additional energy from a source of external periodic force in order to ensure its movement with increasing speed along a trajectory of the unwinding helix type. This movement of the HTSC carrier is due to the vibration of the substrate, in which the MS-4a magnetic system is fixed (see Fig. 8b).

The experiments were carried out at $T \sim 80$ K. The HTSC carrier was placed above the MS-4a magnetic system and set in motion according to the scheme shown in Fig. 8. Freeze-frames of the movement of prototype 2 are shown in Fig. 9. It can be seen that the HTSC carrier, gradually gathering speed, is displaced due to the centrifugal force to the outer boundary of the magnetic system. After reaching a certain speed (the so-called stall speed, v_{out}), which depends on the magnitude and configuration of the magnetic field, as well as on the shape and parameters of the carrier, the HTSC carrier leaves the magnetic system

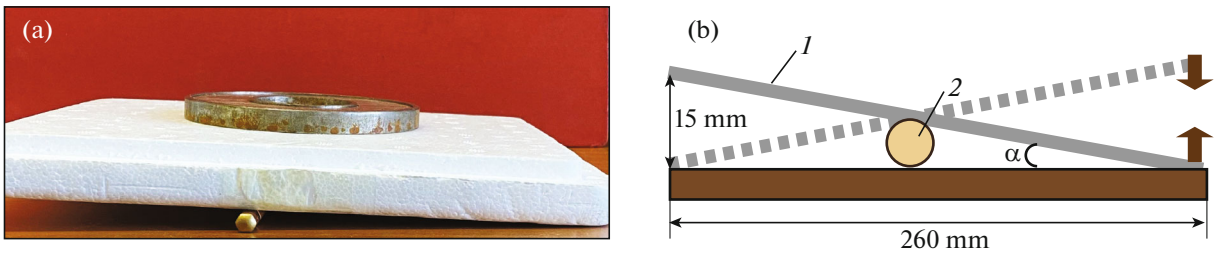

Fig. 8. Setting up an experiment on the acceleration of an HTSC carrier under a variable impact with a frequency of ~1 Hz. (a) General view of the MS-4a system located in a foam plastic substrate and (b) schematic for creating a frequency action (*1* – substrate for fixing MS-4a, *2* – a cylinder with a diameter of 7 mm; the maximum angle of inclination of the substrate $\alpha_{max} = 3.3°$.

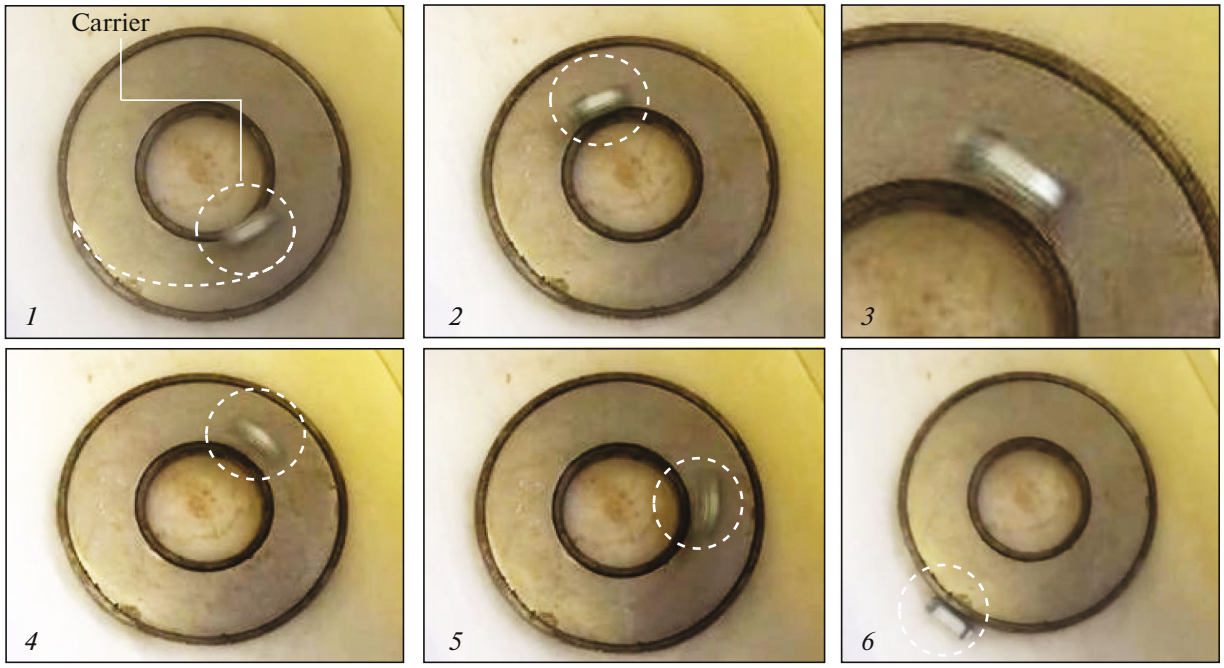

Fig. 9. Freeze-frames of the acceleration of the HTSC carrier (prototype 2) while moving over the MS-4a ring system (frames *1–4*, frame *3* is zoomed in). Upon reaching a certain velocity value (stall velocity v_{out}), the HTSC carrier leaves the circular trajectory tangentially (frames *5* and *6*). In this experiment, $v_{out} = 0.6$ m/s and the levitation height is $h = 8$ mm.

approximately in the middle of the rail along a tangent to the motion trajectory (frames *5* and *6* in Fig. 9). The experimental value of $v_{out}$was determined as a result of frame-by-frame processing of the video recording of the experiment and amounted to 0.6 m/s.

Recall that the gradient of the magnetic field of MS-4a (see Fig. 4, x-component of the field) plays the role of a magnetic wall that holds the HTSC carrier inside the circular magnetic rail until its kinetic energy exceeds the energy of interaction with the magnetic system. The value of the stall velocity is determined both by the properties of the HTSC material (the modulus of M) and by the properties of the magnetic system itself (the value of $K_x = B_x dB_x/dx$); the greater $|M|$, the smaller values of K_x are required to maintain a given speed of the the HTSC carrier. Let us estimate the value of v_{out} based on the measurements performed in this work (see Figs. 2 and 4). The force F_x acting on the HTSC carrier in the x direction (i.e., in this case, along the MS-4a radius) is determined by the formula [19]

$$F_x = \frac{\chi}{2\mu_0} V_s \frac{\partial B^2}{\partial x}, \quad (1)$$

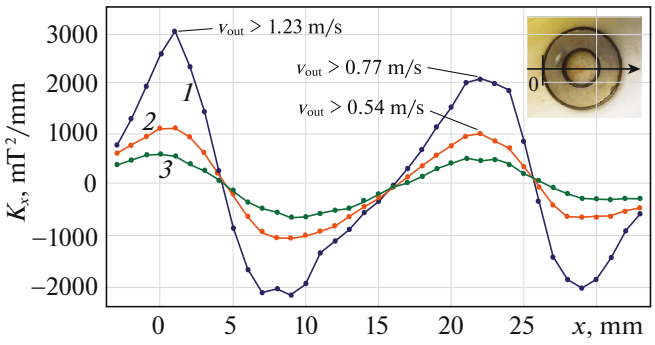

Fig. 10. Calculation of the stalling speed of an HTSC carrier (SuperOx tape) from a circular trajectory for a levitation height h = (*1*) 6, (*2*), and (*3*) 10 mm. Calculation parameters are HTSC tape density $\rho = 3.25$ g/cm^3, $|M| = 0.03$ G · cm^3 at $T = 82$ K, $\eta = 1.04 \times 10^3$ g/cm^3, the x axis is directed along the MS-4a diameter, measured from the outer edge (see inset in the upper right corner); the characteristics of the magnetic field of the MS-4a system are given in Fig. 4.

where μ_0 is the vacuum permeability, χ is the magnetic susceptibility of the HTSC material, V_s is the volume of the carrier, and B is the magnetic induction. To determine χ, we measured the magnetic moment of the HTSC samples $M = \chi H$ on a multifunctional setup PPMS-9 in the ZFC mode (see Section 2.1).

When moving in a circle, the HTSC carrier interacts with the magnetic field of the MS-4a system, creating a force F_x to balance the centrifugal force $F_{cf} = mv^2/R$, where m is the mass of the HTSC carrier and v and R are its velocity and the radius of the trajectory of motion. Using formula (1), the equation of mechanical equilibrium of an HTSC carrier moving along a circular track of the magnetic system takes the form

$$\frac{\chi}{2\mu_0} V_s \frac{\partial B^2}{\partial x} = m\frac{v^2}{R}. \tag{2}$$

Equation (2) can be written in the form convenient for the subsequent analysis:

$$B_x \frac{dB_x}{dx} = \frac{\mu_0}{\chi}\frac{m}{V_s}\frac{v^2}{R}. \tag{3}$$

We introduce a parameter η characterizing the properties of the HTSC material: $\eta = \rho/\chi$, where $\rho = m/V_s$. We rewrite Eq. (3) as follows:

$$K_x = B_x \frac{dB_x}{dx} = \mu_0 \eta \frac{v^2}{R}. \tag{4}$$

The values of η and R determine the value of K_x; i.e., the most important characteristic of the magnetic field along the radius of the magnetic system for each individual value of the velocity v. The results of calculating the velocity v_{out} (Fig. 10) for a certain experimental value of K_x are in good agreement with the experiments on the motion of an HTSC carrier in the MS-4a system (Figs. 9 and 11).

According to calculations for $K_x = 1000$ mT^2/mm and a levitation height of 8 mm, the velocity of departure from the circular trajectory is $v_{out} > 0.54$ m/s and separation occurs at $R \sim 30$ mm; i.e., according to the experiment with prototype 2, approximately at the center of the magnetic rail at $v_{out} = 0.6$ m/s (Fig. 9).

A control series of experiments was carried out for prototype 1 of the HTSC carrier while it was moving at a levitation height of 6 mm. According to the calculations (Fig. 10), for $K_x = 3000$ mT^2/mm and a levitation height of 6 mm in the MS-4a system, the velocity is $v_{out} > 1.23$ m/s when leaving the trajectory along the outer diameter. Experiments with an HTSC carrier fully confirmed the results of the calculation: the measured value of the stall velocity is $v_{out} = 1.38$ m/s (Fig. 11).

Thus, the calculation results are in good agreement with the experimental data for different values of the levitation height of HTSC carriers and the radius of the circular trajectory. The results obtained are summarized in Table 2 (compare the values of v_{out1} and v_{out2}).

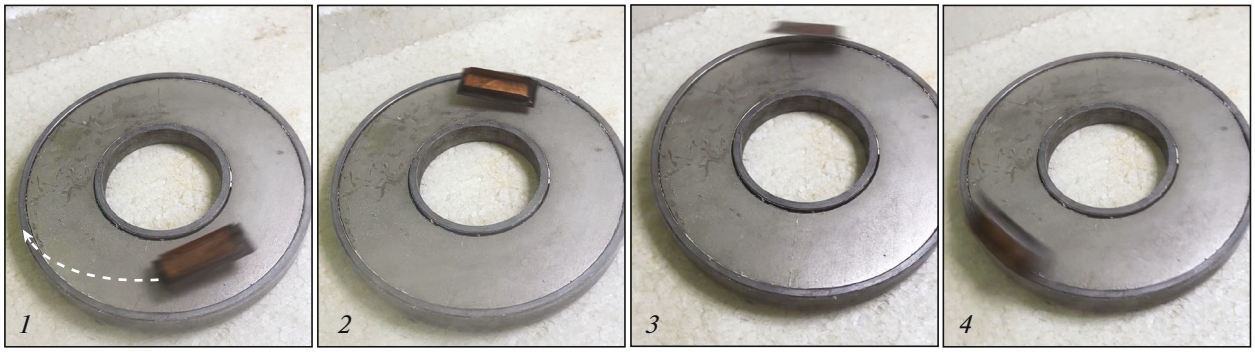

Fig. 11. Acceleration of an HTSC carrier (prototype 1). Freeze-frames of the rotational motion of the HTSC carrier along a changing trajectory at a levitation height of 6 mm: starting from the middle of the MS-4a magnetic system (frame *1*), the HTSC carrier gradually gathers speed and begins to shift towards the outer boundary due to centrifugal force (frame *2*); frames *3* and *4* correspond to the last turn, on which the HTSC carrier leaves the trajectory tangentially to the outer edge of the ring, when its velocity becomes equal to $v_{out} = 1.38$ m/s.

4. DISCUSSION OF THE RESULTS

Let us consider the possibility of transition from prototype experiments to the creation of a prototype ring accelerator for the system of noncontact delivery of CFT to the target chamber of the ICF facility. To do this, let us estimate the value of the injection velocity that can be realized with such an accelerator. Using relation (4), the expression for the velocity can be written as

$$v = \sqrt{K_x \frac{R}{\mu_0 \eta}}. \quad (5)$$

It follows from (5) that, for a given radius R of a ring magnetic system, the greater the velocity v, the smaller the parameter $\eta = \rho/\chi$ and the greater the value of K_x.

To carry out further estimates, we will take into account the range of the values entering into expression (5). First of all, we note the following:

(1) in strong magnetic fields ($B \sim 2$–3 T), the required inhomogeneities on the order of $\partial B^2/\partial x \sim 5 \times 10^2$ T^2/m can be realized at short distances, which limits the size of accelerated bodies to values on the order of several centimeters. Since the diameter of the reactor CFT is ~4 mm [2] and the transverse size of the HTSC carrier does not exceed 1 cm [9], this condition can be easily implemented in practice when constructing a ring accelerator;

(2) currently, superconducting materials with unique properties are being synthesized. For example, several groups of porous superconductors with low density have been studied. The pores in such materials ensure the penetration of coolant, efficient heat dissipation and stable operation of the levitation system. A review of studies of superconductors with a porosity of more than 50% is presented in [20]. These data indicate the possibility of reducing the value of K_x due to a decrease in the density of the HTSC material used to fabricate superconducting carriers of CFTs;

(3) one should also take into account the fact that the CFT accelerator must operate at sufficiently low temperatures, down to 17 K. Measurements of the magnetic moment M performed in this work showed that $|M|$ increases by more than two orders of magnitude as the temperature of the HTSC sample decreases from 85 to 17 K for the range of magnetic fields of our interest ($B \sim 1$–2 T, see Table 1). Let us make estimates for a ring accelerator at $R = 1$ m, $K_x = 500$ T^2/m (which can be written as $K_x = 2$ T $\times$ 0.25 T/mm)

Table 2. Comparative results of modeling the conditions for the stall of an HTSC carrier from a circular trajectory while moving over MS-4a

Experiment (MS-4a system)				Calculation (Fig. 7)
HTSC carrier	h (mm)	R (mm)	v_{out1} (m/s)	v_{out2} (m/s)
Prototype 1 (Fig. 7)	6	50	1.38	$v_{out} > 1.23$
Prototype 2 (Fig. 9)	8	30	1.60	$v_{out} > 0.54$

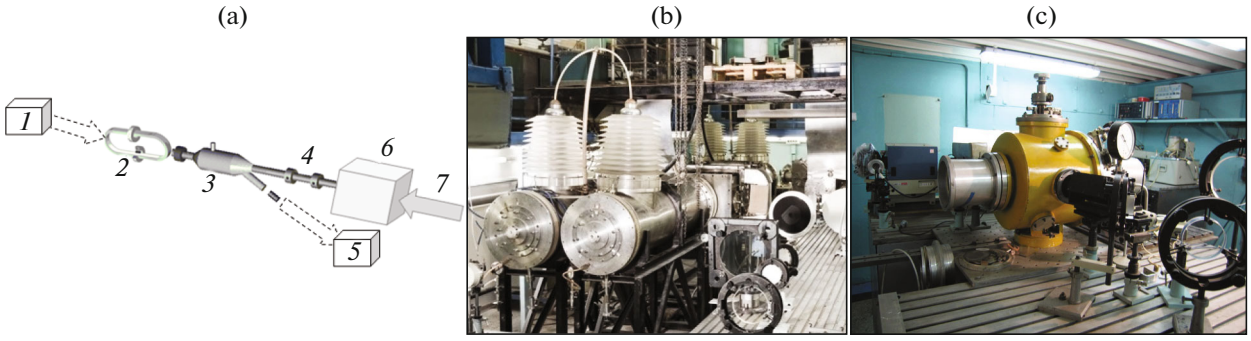

Fig. 12. Noncontact delivery (acceleration + injection) of a surrogate target (ST) to the focus of the GARPUN laser facility: (a) the main elements of the delivery system (*1* – unit for feeding the HTSC carrier + ST assembly into the accelerator; *2* – ring HTSC maglev cyclotron-type accelerator to achieve the required ST injection velocitues; *3* – HTSC carrier and ST separation unit; *4* – system for control of ST parameter, including its trajectory; *5* – unit for storage of spent HTSC carriers; *6* – target chamber (TC); *7* – laser beam of the GARPUN facility), (b) photograph of the GARPUN facility (general view), and (c) photograph of the TC of the GARPUN facility.

and $|M|$ at $T = 17$ K, which is only an order of magnitude higher than in our experiments. In this case, the stall velocity, according to (5), will be ~220 m/s.

Further improvement of the accelerator scheme (a combination of linear and circular tracks when constructing a magnetic system [14, 15]), as well as the choice of promising HTSC materials with a reduced density and high magnetic susceptibility, will make it possible to achieve the required parameters of acceleration of a CFT without stalling of the high-temperature superconductor carrier from the motion trajectory, thereby providing the required CFT injection velocities (200–400 m/s) into the focus of a powerful laser facility or a future ICF reactor.

Note that, in this work, prototype tests were carried out at a temperature not lower than $T = 80$ K and using permanent magnets. In the transition to lower temperatures (when the CFT is accelerated, the operating values are $T \sim 17$ K), it is proposed to use electromagnets wound from a superconducting wire, e.g., from titanium niobate (NbTi), which makes it possible to create fields up to 6–7 T [21, 22], which means that the realization of $B = 1$–2 T will not be a problem. In addition, the use of electromagnets will make it possible, if necessary, to vary the magnetic field profile depending on the CFT acceleration parameters.

5. SPECIFICITIES OF PLANNING A NEW SERIES OF EXPERIMENTS

At the intermediate stage of research, it is planned for the first time to accelerate and inject a surrogate target (ST) into the target chamber of the GARPUN KrF laser (developed at LPI [23]) to realize the synchronous arrival of laser radiation and the injected ST. The acceleration of the ST located inside the HTSC carrier will be provided by a ring HTSC maglev accelerator.

A schematic of the experiment and photographs of the main units of the GARPUN facility operating in the frequency mode are shown in Fig. 12. The analysis of the acceleration process has been discussed in detail in the previous sections. Therefore, below we will dwell on the parameters of the GARPUN facility.

The main wide-aperture amplifier of the GARPUN multistage laser system with an active volume of 15 × 18 × 100 cm and pumping by electron beams was put into operation in 1991 [23]. In the oscillator mode with an optimal unstable cavity with a gain parameter equal to 6, the laser provides an energy of ~100 J in pulses with a duration of 100 ns (peak power ~1 GW), equal to the pump duration. With successive two-pass amplification of pulses from an electric-discharge master KrF oscillator (200 mJ, 20 ns), pulses with an energy of 30 J and a duration of 20 ns (peak power ~1.5 GW) were obtained at the output in a BERDYSh preamplifier with electron-beam pumping and in a final amplifier at the output. With amplification of tripled-frequency subpicosecond pulses of the titanium–sapphire launch complex, pulses with an energy of ~0.6 J and a duration not exceeding 1 ps (peak power of ~1 TW) were obtained at the output of a hybrid system with two wide-aperture amplifiers [24], [25]. Presently, experiments are being carried out at the facility, aimed at reducing the pulse duration of the electric-discharge KrF oscillator for operation in the range from tens to hundreds of picoseconds due to nonlinear optical compression with stimulated scattering and four-wave mixing, as well as at generating 20 ns pulses with a sharp increase in power in last hundreds of picoseconds with simultaneous amplification of long and short pulses in the active medium of a KrF laser [26].

Such pulses are required for a promising ICF scheme with shock ignition of fuel in a precompressed CFT, using a focused shock wave. Within this approach, direct irradiation of CFTs with a low initial aspect ratio are considered, since it is assumed that such CFTs are the most stable during fuel compression in ICF experiments [27]. It is also important that the master oscillator of the GARPUN laser system operates with a laser pulse repetition rate of several Hertz, which will allow for the first time to simulate the possibility of noncontact frequent delivery of STs to the laser focus of the facility by means of an HTSC maglev system.

6. CONCLUSIONS

In this paper, we have presented the results of experimental studies on the acceleration of an HTSC carrier in an HTSC maglev system and carried out theoretical calculations, the results of which are in good agreement with the experimental data. It has been shown that the ability of CFT to withstand thermal and mechanical overloads during its delivery to the reactor chamber can be successfully realized using a new type of accelerator: HTSC maglev in a linear or ring modification with a cyclotron acceleration principle. The advantage here is the noncontact transport and, consequently, the absence of wear and mechanical friction (i.e., the absence of the risk of overheating of the CFT due to the friction of the carrier walls against the accelerator walls). As a result, in the absence of mechanical friction, the issue of developing cryogenic lubricants is removed, the effectiveness of which at temperatures $T < 20$ K is very problematic. All this improves efficiency and reduces maintenance costs, which prolongs the service life of the CFT delivery system, especially when it operates under conditions of fuel injection into the reactor chamber at the required frequency of 5–10 Hz. The results of planning experiments on the acceleration and injection of CFTs into the target chamber of the GARPUN laser facility, developed at the Lebedev Physical Institute, have been presented.

FUNDING

This work was carried out as part of the state order to the Lebedev Physical Institute, Russian Academy of Sciences, and the IAEA (project no. 24154).

CONFLICT OF INTEREST

The authors declare that they have no conflicts of interest.

REFERENCES

1. Goodin, D.T., Alexander, N.B., Besenbruch, G.E., et al., *Phys. Plasmas,* 2006, vol. 13, p. 056305.
2. Bodner, S.E., Colombant, D.G., Schmitt, A.J., and Klapisch, M., *Phys. Plasmas,* 2000, vol. 7, p. 2298.
3. Goodin, D.T., Alexander, N.B., Brown, L.C., et al., *Nucl. Fusion,* 2004, vol. 44, no. 12, p. S254.
4. Baranov, G.D., Koresheva, E.R., Listratov, V.I., et al., USSR Author's Certificate 1586437, 1990.
5. Petzoldt, R.W., Goodin, D., and Siegel, N., *Fusion Technol.,* 2000, vol. 38, no. 1, p. 22.
6. Koresheva, E.R. and Osipov, I.E., USSR Author's Certificate 1820757, 1992.
7. Yoshida, H. and Yamahira, Y., *Laser Original*, 2003, vol. 343.
8. Miles, R., Spaeth, M., Manes, K., et al., *Fusion Sci. Technol.,* 2011, vol. 60, p. 61.
9. Kreutz, R., *Fusion Technol.,* 1988, vol. 8, p. 2708.
10. Aleksandrova, I.V. and Koresheva, E.R., *High Power Laser Sci. Eng.,* 2017, vol. 5, no. 2, p. e11.
11. Koresheva E.R., Aleksandrova I.V., Akunets A.A., et al., RF Patent 2635660, 2017.
12. Aleksandrova, I.V., Akunets, A.A., Koresheva, E.R., and Koshelev, E.L., RF Patent 2727925, 2020.
13. Aleksandrova, I.V., Akunets, A.A., Koresheva, E.R., and Koshelev, E.L., RF Patent 2769777, 2022.
14. Aleksandrova, I.V., Koresheva, E.R., and Koshelev, E.L., *Nucl. Fusion,* 2021, vol. 61, p. 126009.
15. Aleksandrova, I.V., Koresheva, E.R., and Koshelev, E.L., *High Power Lasers Sci. Eng.,* 2022, vol. 10, p. e11.
16. Antonov, Yu.F. and Zaitsev, A.A., *Magnitolevitatsionnaya transportnaya tekhnologiya* (Magnetic Levitation Transport Technology), Moscow: Fizmatlit, 2014.
17. Lee, S., Petrykin, V., Molodyk, A., et al., *Supercond. Sci. Technol.,* 2014, vol. 27, p. 044022.
18. Ginzburg, V.L. and Andryushin, E.A., *Sverkhprovodimost'* (Superconductivity), Moscow: Al'fa-M, 2006.

19. Landau, L.D. and Lifshitz E.M., *Teoreticheskaya fizika. Elektrodinamika sploshnykh sred* (Theoretical Physics. Electrodynamics of Continuous Media), Moscow: Nauka, 1982, vol. 8.
20. Gokhfel'd, D.M., Koblishka, M.R., and Koblishka-Veneva A., *Fiz. Met. Metalloved.,* 2020, vol. 12, p. 1026.
21. Deryagina, I.L., Popova, E.N., and Romanov, E.P., *Vestn. Omsk. Univ.,* 2013, vol. 2, p. 57.
22. Muzzi, L., De Marzi, G., Zignani, C.F., et al., *IEEE Trans. Appl. Supercond.,* 2011, vol. 21, p. 3132.
23. Basov, N.G., Bakaev, V.G., Grigor'yants, E.A., et al., *Sov. J. Quantum Electron.,* 1991, vol. 21, no. 8, p. 816.
24. Zvorykin, V.D., Levchenko, A.O., and Ustinovskii, N.N., *Quantum Electron.,* 2010, vol. 40, no. 5, p. 381.
25. Zvorykin, V.D., Goncharov, S.A., Ionin A.A., et al., *Quantum Electron.,* 2017, vol. 47, no. 4, p. 319.
26. Zvorykin, V.D., Didenko, N.V., Ionin, A.A., et al., *Laser Part. Beams,* 2007, vol. 25, no. 3, p. 435.
27. Shang, W.L., Betti, R., Hu, S.X., et al., *Phys. Rev. Lett.,* 2017, vol. 119, p. 195001.

Translated by E. Chernokozhin